From sample structure to optical properties and back

A theoretical framework for quantitative OCT and its clinical application

Almasian, M.

Publication date
2018

Document Version
Other version

License
Other

CHAPTER 1

INTRODUCTION

The diagnosis of many diseases is based on the analysis of cellular structures of the tissue under study. However, obtaining high resolution images from structures within tissue is hampered by the scattering of light, which limits the imaging depth and blurs the image. The most common clinically applied solution is to take a biopsy and analyzing a thin slice through the microscope. In order to provide microscopic imaging in living tissue, various techniques to circumvent the limitation by scattering have been developed over the years. Optical coherence tomography (OCT) is one of these techniques, which uses near-infrared light to record 3D images of biological tissue with a resolution usually in the range of 5-15 μm, with an imaging depth of approximately 2 mm.[1] The high-resolution is achieved by a detection scheme which combines a confocal gate, and a coherence gate in order to only detect the in focus light at controlled depths in tissue, thereby allowing non-invasive cross-sectional imaging of tissue structure and morphology. In addition to morphological imaging, advanced analysis of the images yields complementary information on microscopic tissue structure and organization not readily visible in the OCT images.[2–4] These tissue properties can be probed by quantification of tissue scattering parameters, which can be extracted from OCT data using an appropriate model for the OCT signal.[5–7] A large number of studies have been dedicated to such quantitative analysis of OCT data to address clinical questions, mostly concerning tissue characterization.[7] Many of these studies on *ex vivo* and *in vivo* tissues show promising results, indicating that these parameters are sensitive to differences in sub-resolution tissue structure and organization.[6] However, the extracted quantitative parameters strongly depend on the applied methodology, and are sensitive to input parameters.[6,7] Currently, there is no consensus on the methodology and the input parameters depend on human choices. In order to determine the clinical value of quantitative OCT, the extracted parameters should be reliable and robust. Furthermore, the sensitivity of these parameters to clini-

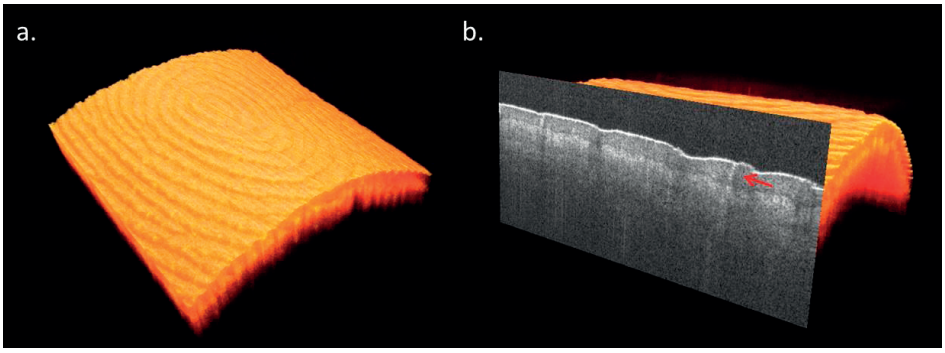

Figure 1. OCT scan of a finger a) 3D view (7 by 7 mm) b) with a cross sectional image. Three tissue layers distinguished in depth: stratum corneum, epidermis, dermis. A sweat gland is depicted by the red arrow. The OCT image was collected using a swept source OCT system with a center wavelength of 1300 nm.

cally relevant changes in tissue should be determined. Therefore, standardization of a validated model describing the OCT signal together with a robust method to extract quantitative parameters is required. Moreover, a theoretical framework is needed to relate these quantitative OCT parameters to clinically relevant tissue properties. This thesis addresses these needs and discusses the possibilities and pitfalls of clinical application of quantitative OCT. Below follows a short introduction of the terminology and concepts of OCT, tissue scattering and quantitative OCT.

OPTICAL COHERENCE TOMOGRAPHY

An OCT system consists of a Michelson (figure 2) or Mach-Zehnder interferometer, which is a beamsplitter that divides the light into two paths: the reference arm and the sample arm.[1] While the light in the reference arm is back reflected by a mirror, the light in the sample arm is partially scattered back due to refractive index variations in the sample. Then, the light from both arms is recombined in the beamsplitter and reflected on to the detector. Because of the low coherence of the light source, interference between the back reflected light of the reference arm and sample arm occurs when the path length in both arms is matched within the coherence length. Hence, of all the backscattered light OCT is exquisitely sensitive to light which has undergone one or a few scattering events.[1,4] The coherence length defines the axial resolution of the OCT system and is given by[1]:

$$\Delta z = \frac{2ln2}{n\pi} \frac{\lambda_0^2}{\Delta\lambda} \tag{1}$$

where Δz is the coherence length, n is the refractive index, λ_0 is the center wavelength and $\Delta\lambda$ is the bandwidth of the illumination source.

A depth profile (A-scan) of the sample is constructed based on the traveled path length of the detected light. Lateral scanning of the beam over the sample then allows construction of 2D (B-scan) and 3D (C-scan) images of the tissue under study. Measurement of a sequence of A-lines in time at the same location (M-mode scan) enables time-resolved measurements. The lateral resolution of an OCT system is defined by the sample arm optics. The imaging depth is determined by the illumination and detection specifications, but is usually limited by wavelength dependent scattering by the sample.[1] In general larger imaging depths can be achieved by longer wavelengths. To maximize imaging depth commonly used OCT wavelengths (around 850, 1050, and 1300 nm) are within the tissue optical window, a range of wavelengths in which light absorption in living tissues is relatively low.

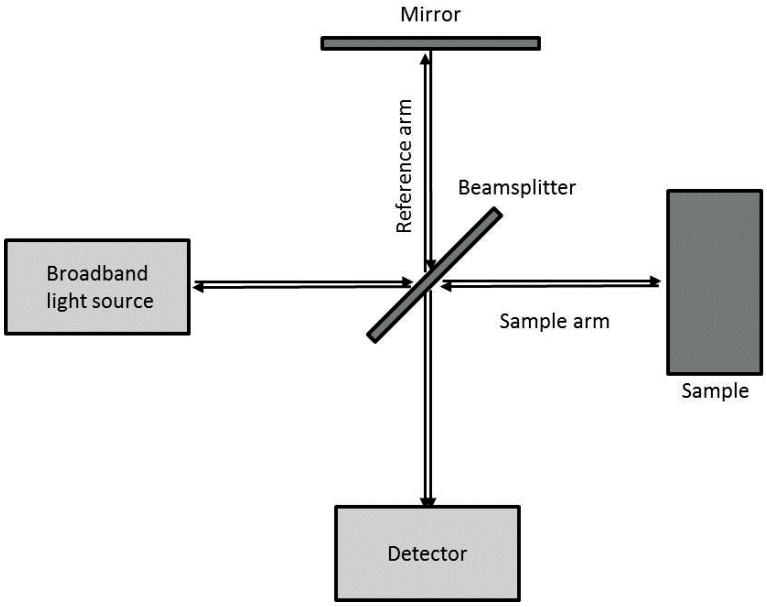

Figure 2. Schematic view of a Michelson interferometer. The light from a broadband low-coherence light source is divided by the beamsplitter in two paths i.e. the reference arm and the sample arm. The back reflected light from both arms is then recombined by the beamsplitter, where after the interference of the light between these two arms is measured by the detector.

CLINICAL APPLICATION

OCT straddles the imaging resolution range between microscopy and clinical imaging techniques such as ultrasound, MRI and CT. Due to its high resolution, non-invasive, contact- and label-free imaging capabilities, OCT is well suited for clinical and intra-operative use.[14] Moreover, its imaging speed enables collection of 3D data sets within seconds, limiting the influence of motion artifacts induced by heartbeat and respiration. To overcome the limited penetration depth in tissue, catheter-based and needle-based OCT probes have been developed to enable minimally invasive imaging inside the human body.[15–17] Images of tissue morphology have been successfully collected both *ex vivo* and *in vivo,* of various human organs, including the retina, coronary artery, gastric tract, urinary tract, prostate, breast, and brain. OCT has been adopted as a routinely used clinical tool in two medical fields. In ophthalmology OCT is used in daily practice to visualize the retina, cornea, retinal vasculature, and pre- and postoperatively in retinal surgery;[14] cardiological OCT is mainly used to visualize surgical implanted stents inside the coronary arteries.[18] Other imaging applications such as that of (epithelial) tumors and vascular plaques are being explored in pre-clinical studies.[7] Furthermore, studies towards the clinical use of quantitative OCT are being pursued to obtain additional information

on microscopic tissue properties not readily visible in the OCT images.[7] Microscopic tissue properties such as structure, organization and flow determine tissue scattering properties. This relationship can potentially be used to address important clinical questions concerning e.g. tissue characterization, grading of cancerous lesions and detection of (blood) flow; as the structure and organization of tissue are altered due to disease, pathological changes in tissue could be probed by determination of tissue scattering properties. Experimental evidence shows that subtle changes between pre-invasive cancer cells compared to normal cells,[19] and for apoptotic compared to necrotic cells[20] can be detected through the measurement of sample scattering properties.

SCATTERING PROPERTIES

Scattering of light by tissue is determined by the spatial variation of the refractive index which in turn is a result of tissue structure and organization. The variation of refractive index in tissue is known to exhibit fractal properties because of the wide range of scatterer sizes present in the tissue.[21–24] Scattering properties are commonly expressed in terms of the wavelength dependent scattering coefficient (μ_s) in mm^{-1} and phase function ($P(\theta)$).[25] The scattering coefficient quantifies the probability of scattering per unit length. The multiplicative inverse of the scattering coefficient ($1/\mu_s$) therefore defines the average path length light can travel in a medium without scattering. The phase function expresses the probability of scattering per unit angle. A measure of the phase function is usually given by the anisotropy factor (g), which is the average cosine of the scattering angle ($<\cos(\theta)>$). g has values between -1 and 1, where g = -1 corresponds to full backward scattering and g = 1 corresponds to full forward scattering. Furthermore the backscattering coefficient (μ_B) can be defined, which is the light scattered back under an angle of 180° with respect to the direction of the incident light.[25] In practice, backscattered light is measured within a finite numerical aperture, so that a backscattering coefficient $\mu_{B,NA}$ can be defined which accounts for light scattered within the NA around 180 degrees. For individual spherical particles Mie-theory can be used to calculate scattering properties i.e. scattering cross section (σ_s) and the phase function ($P(\theta)$) as functions of particle size, refractive index mismatch of the particle and the surrounding medium, and the illumination wavelength.[25] The scattering cross section expresses the loss of energy from the incident beam due to scattering by a particle in area dimensions (mm^2). For dilute solutions μ_s is obtained by multiplying σ_s with particle concentration. For non-dilute higher particle concentrations (>2 volume %), the calculation of μ_s can be augmented by the Percus-Yevick structure factor, to include particle organization in the description of scattering behavior.[26]

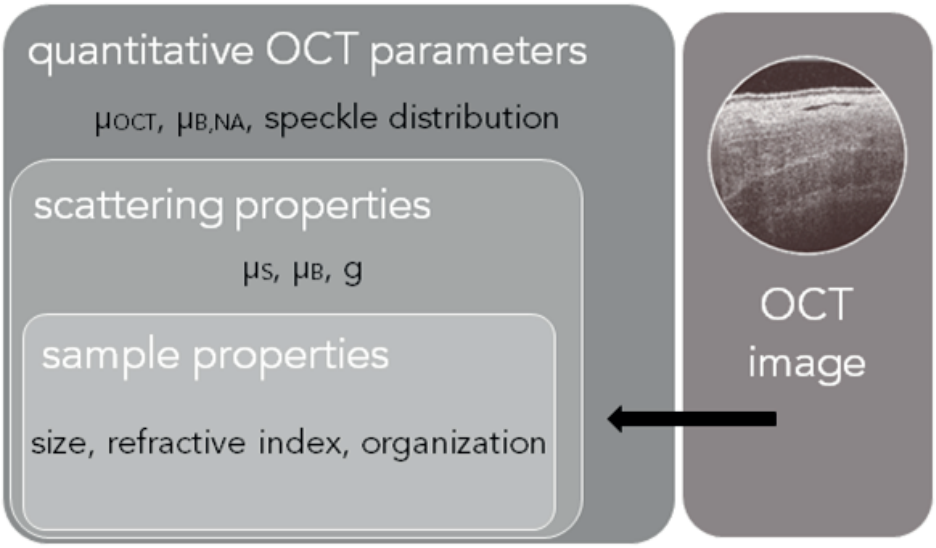

Figure 3. A schematic overview of the relation between the OCT image, quantitative OCT-parameters, scattering properties and sample properties. Please note that this scheme only includes scattering and does not include absorption.

QUANTITATIVE OCT PARAMETERS

As discussed above tissue structure and organization can be probed by scattering properties. These, in turn can be accessed by extracting quantitative parameters from OCT data, such as amplitude, attenuation coefficient and speckle distribution (figure3). Perhaps the most accessible and researched quantitative parameter in OCT is the attenuation coefficient, describing the decrease of the OCT signal in depth, for which the symbol μ_t is often used. μ_t is formally defined as: $\mu_t = \mu_s + \mu_a$, and is equal to μ_S in the case of exclusively single scattered light and known absorption coefficient.[6] However, because this is not always the case in OCT we use the notation μ_{OCT} instead of μ_t. Additionally, the backscattering coefficient $\mu_{B,NA,}$ which is the backscattered signal integrated over the detection numerical aperture of the system, can be extracted from the OCT amplitude after careful calibration.[6] In order to extract $\mu_{B,NA}$ and μ_{OCT} from OCT data, multiple models describing the OCT signal have been developed.[4,6,7] The most commonly used model is based on the first order Born approximation, which assumes that the field inside the scattering volume is equal to the incident field; the OCT signal amplitude as a function of depth in a homogeneous turbid medium is then usually described as a single exponential decay, assuming the detected backscattered light has only interacted with the sample in one scattering event. Further, omitting noise terms, the mean OCT amplitude at depth *z* is expressed as[6]:

$$\langle A(z)\rangle \propto \sqrt{\mu_{B,NA}}\, exp(-\mu_{OCT}(z)) \quad (2)$$

where, $A(z)$ is the OCT signal amplitude; $\mu_{B,NA}$ is the backscattering coefficient; and μ_{OCT} is the attenuation coefficient. Please note that Eq. (2) does not take into account system dependent influences on the signal, which will be discussed in detail in the following chapters in this thesis. In addition to $\mu_{B,NA}$ and μ_{OCT}, studies suggest that statistical measures of the speckle pattern in OCT images can be quantified as an additional parameter to derive sub-resolution structural tissue properties, and potentially provide a tool for tissue characterization in the clinic.[27,28] In OCT, speckle is the voxel-to-voxel fluctuation of the OCT amplitude caused by phase differences of the backscattered field due to the spatial distribution of the scattering particles in the sample.[22,29] Hence, speckle contains information on the scattering particles that are in general smaller than the OCT resolution. Speckle-based flow measurements (e.g. in flow channels or blood vessels) have shown promising results. Studies have established the relation between OCT speckle and flow in the imaged sample, ranging from qualitative detection of flow in order to visualize blood vessels, to quantitative analysis of flow velocity in controlled measurement settings.[30–35]

AIM AND OUTLINE OF THIS THESIS

The aim of this thesis is to derive and validate a model describing the OCT signal, to provide a robust method to extract quantitative parameters (amplitude, attenuation coefficient and speckle distribution) from OCT data, and to relate these parameters to sample properties (structure, organization and flow). In the first part of this thesis we derive and validate a model for the OCT signal for mono-disperse and homogeneous discrete random media (DRM). DRM are randomly positioned identical spherical particles for which calculations of the scattering properties are straightforward, thereby allowing the accurate study and separation of the influence of sample properties and system properties on the OCT signal. As an experimental equivalent of DRM we use suspensions of silica microbeads in water to create samples with controlled properties (size, refractive index and concentration). By using differently sized silica microbeads at different concentrations we are able to generate samples covering a large range of optical properties. In the latter part of this thesis, the findings of the first two chapters are applied in two *in vivo* pilot studies investigating the feasibility of (intraoperative) quantitative OCT during surgery. These two clinical applications are examples where non-invasive intraoperative imaging could be a powerful and valuable aid to the surgical practice. The content of each chapter in this thesis is discussed briefly below.

Chapter 2 describes a theoretical derivation of the OCT signal amplitude and speckle distribution for mono-disperse and homogeneous DRM, assuming single scattering. This

chapter provides a theoretical framework relating sample properties (particle size and concentration) to OCT scattering parameters ($\mu_{B,NA}$, μ_{OCT} and speckle variance). **Chapter 3** presents a comprehensive approach enabling extraction of $\mu_{B,NA}$ and μ_{OCT} from OCT data of mono-disperse and homogeneous DRM over a large range of scattering properties. Here, the influence of multiple scattering is taken into account by using the Extend-Huygens Fresnel model for OCT in conjunction with a priori knowledge of sample properties. In both studies, model-based predictions are validated with experimentally obtained OCT scattering parameters from silica microbeads in water. **Chapter 4** is a review of the literature on available models and methods to extract μ_{OCT} from OCT data, and an overview of μ_{OCT} values obtained in (pre-)clinical studies. **Chapter 5** investigates the feasibility of *in vivo* quantitative OCT during brain tumor resection surgery, with the ultimate aim of differentiating glioma tissue from normal brain tissue by μ_{OCT}. In **chapter 6** speckle contrast of M-mode OCT scans is used as a tool to detect blood vessels in *in vivo* OCT images collected during reconstructive gastric surgery, by distinguishing areas with flow from the surrounding static tissue. . In both chapter 5 and 6, a robust and validated data analysis pipeline is developed to automatically extract parameters from OCT data. Finally, in **chapter 7**, the most important findings of this thesis are discussed followed by suggestions for future research.

REFERENCES

1. Drexler, Wolfgang, and James G. Fujimoto, eds. *Optical coherence tomography: technology and applications*. (Springer Science & Business Media, 2008).
2. Schmitt, J. M. Optical Coherence Tomography (OCT): A Review. *IEEE J. Sel. Top. Quantum Electron.* **5,** 1205–1215 (1999).
3. Schmitt, J. M., Knuttel, A., Yadlowsky, M. & Eckhaus, M. A. Optical-coherence tomography of a dense tissue: statistics of attenuation and backscattering. *Phys. Med. Biol.* **39,** 1705 (1994).
4. Schmitt, J. M., Knuttel, A. & Bonner, R. F. Measurement of optical properties of biological tissues by low-coherence reflectometry. *Appl. Opt.* **32,** 6032–6042 (1993).
5. Schmitt, J. M. & Knüttel, A. Model of optical coherence tomography of heterogeneous tissue. *J. Opt. Soc. Am. A* **14,** 1231–1242 (1997).
6. Almasian, M., Bosschaart, N., van Leeuwen, T. G. & Faber, D. J. Validation of quantitative attenuation and backscattering coefficient measurements by optical coherence tomography in the concentration-dependent and multiple scattering regime. *J. Biomed. Opt.* **20,** 121314-1-121314–11 (2015).
7. Almasian, M. *et al.* Parametric imaging of attenuation by optical coherence tomography: A review of models, methods and clinical applications. *[SUBMITTED]*
8. Yang, Y. *et al.* Optical scattering coefficient estimated by optical coherence tomography correlates with collagen content in ovarian tissue. *J. Biomed. Opt.* **16,** 090504-1–3 (2011).
9. Wessels, R. *et al.* Optical coherence tomography in vulvar intraepithelial neoplasia. *J. Biomed. Opt.* **17,** 116022-1-116022–6 (2012).
10. Soest, G. Van *et al.* Atherosclerotic tissue characterization in vivo by optical coherence tomography attenuation imaging. *J. Biomed. Opt.* **15,** 011105-1–9 (2010).
11. Scolaro, L. *et al.* Parametric imaging of the local attenuation coefficient in human axillary lymph nodes assessed using optical coherence tomography. *Biomed. Opt. Express* **3,** 366–379 (2012).
12. McLaughlin, R. A. *et al.* Parametric imaging of cancer with optical coherence tomography. *J. Biomed. Opt.* **15,** 046029-1-046029-4 (2010).
13. Xie, T., Zeidel, M. & Pan, Y. Detection of tumorigenesis in urinary bladder with optical coherence tomography: optical characterization of morphological changes. *Opt. Express* **10,** 1431–1443 (2002).
14. Carrasco-Zevallos, O. M. *et al.* Review of intraoperative optical coherence tomography : technology and applications [Invited]. *Biomed. Opt. Express* **8,** 1607–1637 (2017).
15. Kirtane, T. S. & Wagh, M. S. Endoscopic optical coherence tomography (OCT): Advances in gastrointestinal imaging. *Gastroenterol. Res. Pract.* **2014,** (2014).
16. D'Hooghe, J. N. S. *et al.* Optical coherence tomography for identification and quantification of human airway wall layers. *PLoS One* **12,** 1–13 (2017).
17. McLaughlin, R. A. *et al.* Imaging of breast cancer with optical coherence tomography needle probes: Feasibility and initial results. *IEEE J. Sel. Top. Quantum Electron.* **18,** 1184–1191 (2012).
18. Bouma, B. E. *et al.* Evaluation of intracoronary stenting by intravascular optical coherence tomography. *Heart* **89,** 317–320 (2003).
19. Backman, V. *et al.* Detection of preinvasive cancer cells. *Nature* **406,** 35–36 (2000).

20. van der Meer, F. J. *et al.* Apoptosis- and necrosis-induced changes in light attenuation measured by optical coherence tomography. *Lasers Med. Sci.* **25,** 259–267 (2010).
21. Cheong, W. F., Prahl, S. A. & Welch, A. J. A review of the optical properties of biological tissues. *iEEE J. Quantum Electron.* **26,** 2166–2185 (1990).
22. Rogers, J. D., Radosevich, A. J., Yi, J. & Backman, V. Modeling Light Scattering in Tissue as Continuous Random Media Using a Versatile Refractive Index Correlation Function. *IEEE J. Sel. Top. Quantum Electron.* **20,** (2014).
23. Schneiderheinze, D. H. P., Hillman, T. R. & Sampson, D. D. Modified discrete particle model of optical scattering in skin tissue accounting for multiparticle scattering. *Opt. Express* **15,** 3051–3053 (2007).
24. Jacques, S. L. Optical properties of biological tissues: a review. *Phys. Med. Biol.* **58,** R37–R61 (2013).
25. van der Hulst, H. C. *Light Scattering by Small Particles.* (Dover publications, New York, 1957).
26. Nguyen, V. D., Faber, D. J., van der Pol, E., van Leeuwen, T. G. & Kalkman, J. Dependent and Multiple Scattering in Transmission and Backscattering Optical Coherence Tomography. *Opt. Express* **21,** 29145–29156 (2013).
27. Lindenmaier, A. A. *et al.* Texture analysis of optical coherence tomography speckle for characterizing biological tissues in vivo. *Opt. Lett.* **38,** 1280–1282 (2013).
28. Danilo, A. J. & Iskander, D. R. Assessment of corneal properties based on statistical modeling of OCT speckle. *Biomed. Opt. Express* **8,** 461–469 (2017).
29. Schmitt, J. M., Xiang, S. H. & Yung, K. M. Speckle in optical coherence tomography. *J. Biomed. Opt.* **4,** 95–105 (1999).
30. Jansen, S. M. *et al.* Applicability of quantitative optical imaging techniques for intraoperative perfusion diagnostics : a comparison of laser speckle contrast imaging , sidestream dark-field microscopy , and optical coherence tomography. *Jounal Biomed. Opt.* **22,** 086004-1-086004-9 (2017).
31. Gong, P. *et al.* Optical coherence tomography for longitudinal monitoring of vasculature in scars treated with laser fractionation. *J. Biophotonics* **6,** 626–636 (2016).
32. Mariampillai, A. *et al.* Optimized speckle variance OCT imaging of microvasculature. *Opt. Lett.* **35,** 1257 (2010).
33. Weiss, N., Leeuwen, T. G. Van & Kalkman, J. Localized measurement of longitudinal and transverse flow velocities in colloidal suspensions using optical coherence tomography. *Phys. Rev. E* **042312,** 1–7 (2013).
34. Mahmud, M. S. *et al.* Review of speckle and phase variance optical coherence tomography to visualize microvascular networks. *J. Biomed. Opt.* **18,** 50901 (2013).
35. Mariampillai, A. *et al.* Speckle variance detection of microvasculature using swept-source optical coherence tomography. *Opt. Lett.* **33,** 1530–1532 (2008).